https://doi.org/10.2352/ISSN.2169-4451.2019.35.152

IMAGE-BASED NON-CONTACT CONDUCTIVITY PREDICTION FOR INKJET PRINTED ELECTRODES*

Yang Yan, Qingyu Yang, Kerry Maize, Jan P. Allebach, Ali Shakouri, George T. Chiu; Purdue University; West Lafayette, Indiana, United States

Abstract

Inkjet printed electrodes based on metal nanoparticle inks represent a significant component in low cost, thin film electronics. When scaled to continuous reel-to-reel processing platforms, there is an advantage in non-contact, imaging-based methods to monitor the quality of inkjet printed structures in real time. We developed a machine learning method to predict inkjet printed electrode sheet resistance based on microscope images of the device. The method can be extended to nondestructive, uninterrupted quality monitoring many reel-to-reel thin film manufacturing applications.

Strips of silver nanoparticle electrodes are systematically printed with different inkjet print parameters such as ink drop size and drop spacing. Then, a machine learning model is trained on processed microscope images of the electrodes and experimentally measured electrode sheet resistance. The resulting model can predict sheet resistance from images of the electrode with error as small as 10%.

Motivation

The performance of inkjet printed electrodes can vary greatly depending on print parameters. In scalable manufacturing scenarios, such as reel-to-reel inkjet printing, device yield is highly sensitive to process conditions and it is important to monitor quality of printed structures in real time. A primary performance metric for a thin film electrode is minimizing sheet resistance. Toward this goal, we developed an in-situ, noncontact machine learning method to predict sheet resistance of silver nanoparticle inkjet printed electrodes based on topological features visible in microscope images of the electrode.

Problem

Clogged printheads, incorrect or inconsistent drop size, drop spacing, ink dilution, substrate temperature, and other inkjet print conditions can result in nonuniform distribution of the conducting material. Surface roughness, gaps, ridges, pooling, and overspreading of the metal nanoparticle ink degrades conductance. In this study we demonstrate correlation between topological defects visible in microscope images of the electrodes and increased electrode sheet resistance. A machine learning model trained on data sets consisting of measured electrode sheet resistance and microscope images is shown to predict sheet resistance based solely on images of the electrodes with an average accuracy of 26%.

The original design of these printed electrodes was for manufacturing of Nitrate sensors. To construct Nitrate sensors, a transparent ion select membrane is coated on top of the silver electrodes. The smoothness of the surface of the electrodes will affect the thickness and integrity of the top coating layer. Direct contact in-situ measurements can damage the sample or reduce manufacturing speed in reel-to-reel fabrication. Therefore non-contact quality assessment such as image based methods provide significant advantages in reel-to-reel settings. Although the method demonstrated here used single sheets of electrodes printed on a table top inkjet printer, the method can be adapted to near real time quality prediction for inline reel-to-reel processing. Using a machine learning method, the sheet resistances of the printed electrodes are predicted with the features extracted from images of the electrodes.

*Research supported by the SMART Films consortium (https://engineering.purdue.edu/SMART-consortium).

Approach

The proposed method for predicting the sheet resistance of inkjet printed silver electrodes is based on an experimental sheet resistance measurement made physically on the electrodes and the features extracted from digital images of the measured region. In the model fitting process, the prediction model is trained with the features extracted from the digital images as inputs and measured sheet resistance as outputs. Finally, the sheet resistance of the printed silver electrodes can be predicted by using just the images of the electrodes. This image-based and experiment-based method is highly reliant on a systematic printing process and consistency of the inkjet printer operation.

Experiments and Data Collection

The silver electrodes are systematically printed with different ink drop size cartridges (1 pL/10 pL) and drop spacing with the same silver nano-particle ink with 3% Ammonium Carbamate[1] loading using a FUJI Film Dimatix Inkjet printer (FUJIFILM Dimatix Materials Printer DMP-2800 Series). The printing plan is shown in Table 1. At least 20 of the electrodes are printed on one sheet with the parameter values specified in each row. The time consumed for printing one sheet of electrodes usually ranges from 1 hour to 10 hours according to its drop spacing. The smaller the drop spacing is, the more time is required. A whole sheet of printed electrodes and dimensions of one electrode is shown in the Figs. 1 and 2.

Table 1: Printing Plan

Ink Drop Size (10 pL/1 pL)	Ink Drop Space (μm)
10 pL	40 (635 dpi)
	25 (1016 dpi)
	20 (1270 dpi)
1 pL	25 (1016 dpi)
	20 (1270 dpi)
	10 (2540 dpi)

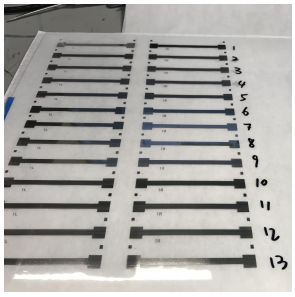

Figure 1. *Sample of Printed Electrodes For One Set of Parameter Values*

To collect the data, sheet resistance of each of the electrodes is taken at five positions for each electrodes using a Jandel multi-height probe as shown in Figure 2.The device is designed to perform multiple electrical measurements for samples with varying thicknesses. Each sheet resistance measurement takes about 50 seconds to 5 minutes.The sheet resistance measurement results of all 120 electrodes are shown in Figure 3. The boxes are the average value plus or minus the standard deviation of the five sheet resistance measurements for one electrode, while the whiskers are the maximum and minimum measurement values among the five sheet resistances. Sheet resistance values are plotted on log scale to show the large variation produced by systematically changing inkjet print parameters.

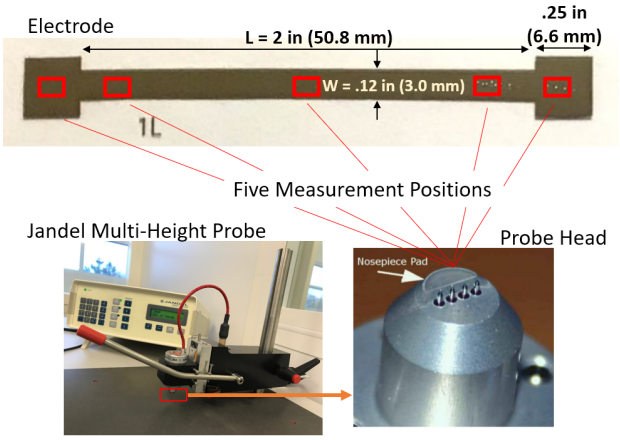

Figure 2. *Electrode Dimensions and Sheet Resistance Measurement Positions*

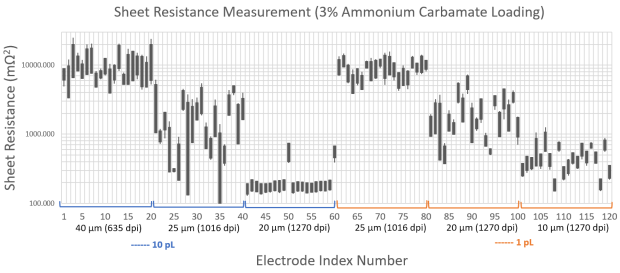

Figure 3. *Sheet Resistance Measurement Results for Silver Nano-particle Ink with 3% Ammonium Carbamate Loading, 10/1 pL Ink Drop Size from 40 µm to µm*

On the same area where the sheet resistance measurement is taken, digital images are captured with a 0.5× magnification telecentric lens (Edmund Techspec compact telecentric lens # 63-741), an in-line light source (Fiber-Lite PL900 illuminator), and a progressive scan CMOS camera (Edmund EO1312 Color USB 3.0 Camera with a 2400 ppi resolution color CCD sensor). Due to the transparency of the substrate, a piece of silicon wafer is put beneath the imaging area to remove the noise generated by the surface of imaging system operating platform.

Features Extraction

Since the light intensity over the image is not evenly distributed, before any image analysis techniques are applied to the images, flat field correction[2] is applied to all of the images. The dark field image (D in Equation 1) is taken when the lens is covered and the resulting image of the camera used here is completely dark with 0 values across the whole image. Several flat field images (F in Equation 1) are captured when the settings of the light and camera are the same as those when images (R in Equation 1) to be corrected are captured. The comparison between the raw image and the corrected image is shown in Figure 4.

$$
\begin{aligned}
C &= (R-D)\times\frac{m}{F-D} = R\times\frac{m}{F} \\
m &= \frac{\sum_{i=1}^{M}\sum_{j=1}^{N}F(i,j)}{M\times N} \\
&where \quad M = image\,width,\ N = image\,length, \\
&(i,j) = pixel\,position
\end{aligned}
\tag{1}
$$

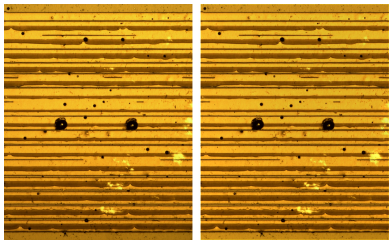

Figure 4. *Before (Left) and After (Right) Flat Field Correction Applied to the Image of the Electrode Printed with 10 pL, 25 µm drop size (1016 dpi)*

The two dark circles on the image are dents left by the middle two probes' head of the Jandel when doing the sheet resistance measurement. The variations in image intensity and colors for the horizontal ink lines is caused by a varying number of print passes. This was confirmed by printed electrodes height analysis performed using 3-D optical profilometer (Zeta-20). Strips with darker color are areas that were covered with doubled layers of ink. And some of the very narrow strips are areas that are not covered by any ink. Uniformity and thickness of the printed ink is a great factor impacting the conductivity. Thus, for a given electrode the ratios of single layer, double layer, or no ink, greatly affect sheet resistance, and these ratios can be extracted from their relative color intensity in the microscope image.

The first step of the segmentation is to separate the electrode area and the background area (Figure 5). The flat field corrected RGB images are converted to grayscale images. Sobel edge detector[3] and Otsu's method[4] are applied to the grayscale images sequentially. The background and the electrode area is

cropped with the most outer edge pixels shown in image [3] of Figure 5.

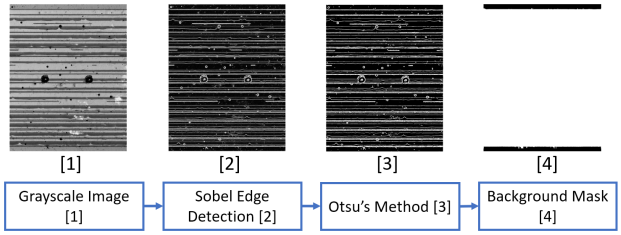

Figure 5. *Background Subtraction*

To subtract the single and double layer ink areas and background areas, the resulting image from the third step ([3] in Figure 5) is inverted and masked with the background mask ([4] in Figure 5). The K-means clustering[5][6] training method is applied to the pixels of the inverted and masked image. The connected components are identified as either double layered ink areas or no ink areas according to their pixel distribution in 3 clusters. The final segmentation result is shown [7] in Figure 6. The single layer, double layer, and no ink areas are segmented correctly, except that the strip located in the center is mistakenly segmented as a no ink area. This is due to the circular dents left by the sheet resistance measurement probe heads.

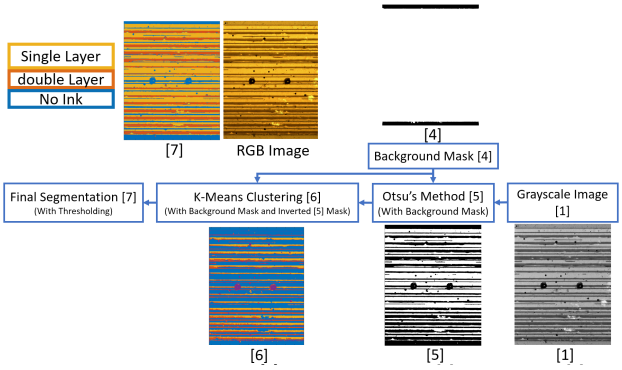

Figure 6. *Image Segmentation Process*

After the segmentation, the proportions of each segmentation area within the electrode area are calculated based on the image [7] in Figure 6. And the average light intensity for each segmentation area is calculated based on both the image [7] in Figure 6 and the Y values, which represent the relative luminance for each pixel of the flat field corrected image in the CIE XYZ color space[7].

The edge raggedness of the electrode's top and bottom edges are calculated, which are specified in the background mask image ([4] in Figure 5 or Figure 6). The edge raggedness is the geometric distortion of an edge from ideal. Simple linear regression is applied to the positions of the edge pixels to form a fitted line. The raggedness is calculated as the standard deviation of the residuals of the actual contour to the fitted line[8] (Equation 2).

$$Edge\ Roughness(ER) = \sqrt{\frac{\sum_{i=1}^{M}\left[Fitted\ line(i) - Data(i)\right]^2}{M}},$$
$$where \quad M = image\ width\ i = pixel\ horizontal\ position \tag{2}$$

Several methods were used to assess electrode surface roughness from the images. The most straightforward method is edge proportion (EP) method. The edge proportion is the ratio of the number of edge pixels to the total number of pixels in the electrode area. This EP is calculated based on the binary images [3] and [4] in Figure 5.

Non-uniformity in the structures can appear with many different dimensions, and it is difficult to say whether a deep pinhole or a big, but shallow dent with larger roughness has more impact on the sheet resistance measurement. With the Gaussian pyramid[9] technique, the surface roughness on a variety of scales can be collected. As shown in Figure 7, the original image is the Layer 0 in the Gaussian pyramid. The standard deviation of the Y values of the upsampled images belonging to each layer of the Gaussian pyramid is calculated, and serves as one of the features representing the unevenness of the surface.

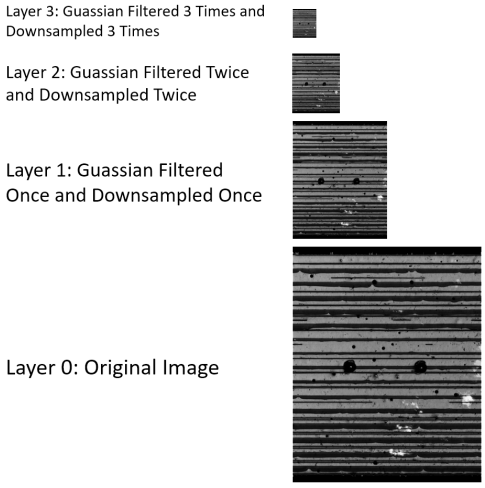

Figure 7. *Gaussian Pyramid*

Another technique called local binary pattern[10] (LBP) is well known for its light independence and wide applications in characterizing texturing of paper[11] and in the computer vision for face detection[12]. This technique is also applied here to provide more information about the texture of the printed electrode surface. The local binary pattern used here is a rotation invariant method with circular operators. With this method, the output of the local binary pattern with eight neighbours is a 10-element array to represent the local texture.

Model Fitting and Cross Validation

All the features extracted from images of the inkjet printed silver electrodes are merged into one matrix with a total of 19 columns and 600 rows as an input matrix for the training model.

The input matrix contains five columns for the image segmentation and 14 columns for surface roughness. Since 20 electrodes are printed for each of six sets of printing parameters and each electrode has five sheet resistance measurements and five matched images, the total number of rows for the input matrix sums to 600. For the same reason, the output matrix, which is the sheet resistance measurement data for each measuring position has 600 rows. One model is trained for each set of printing parameters. In total, six models are trained.

Before the model fitting process, all of the data need to be normalized. After normalization, all the data have been scaled to the range from 0 to 1. All the features extracted from images are normalized with the min-max normalization method and the sheet resistance measurement data is normalized with a logarithm normalization method (Equation 3).

$$\begin{aligned} Normalized\,Data &= \frac{Data - min(Data)}{max(Data) - min(Data)} \\ R_u &= \frac{log_{10}R}{log_{10}[max(R)]} \end{aligned} \tag{3}$$

Two regression training models have been tested separately for the model fitting process: the least squares[13][14] (LSQR) method and the support vector machine regression[15] (SVM Regression) method. Both the least squares regression method and the support vector machine regression method are trained with all the data and tested on the same data. The output of the test step is the predicted electrode sheet resistance based on the microscope images. The average $\bar{R}_{Exp}$ of the five experimental sheet resistance measurements for each electrodes is calculated to represent the print quality for the whole electrode. And the average $\bar{R}_{Pred}$ of the five predicted sheet resistances is calculated in the same way.

The root mean square error (RMSE) in percentage units is used here to to evaluate the goodness of fit for regression training models. Therefore, the RMSE value quantifies the accuracy of our predicted electrode sheet resistance. The calculation of RMSE in percentage is based on the average experimental sheet resistance measurements $\bar{R}_{Exp}$ and the average predicted sheet resistance for each electrodes $\bar{R}_{Pred}$ (Equation 4).

Because the two regression models produce very similar model fitting and cross-validation results, here only the result produced by the least square methods will be presented.

$$\begin{aligned} &RMSE(\%) \\ &= \sqrt{\frac{1}{N}\sum_{index=1}^{N}\left[\frac{|\,\bar{R}_{Pred}(index) - \bar{R}_{Exp}(index)\,|}{\bar{R}_{Exp}(index)}\right]^2} \times 100\% \\ &where \quad N = total\,No.\,of\,electrodes \end{aligned} \tag{4}$$

Five-fold cross validation is performed to assess the prediction accuracy of the models. For one test, the 120 electrodes are divided into five groups randomly. Every group has four electrodes that are printed with the same set of parameters. With six sets of printing parameters, the number of electrodes for each group sums to 24. One at a time, each of the five groups serves as a test set and the remaining four groups are the training set. After performing these five tests, the 120 electrodes are reformed randomly into five new groups serving for the next set of five tests. The total number of test iterations is 100, which means the 120 electrodes are reformed 100 times and each electrodes is tested 100 times. The final test error for each electrode is the average value across the 100 tests. Because the final test error for each page is based on multiple repetitions of the training process with randomly formed data sets, the final test error (Equation 5) is also called average absolute relative error (Avg.Abs.Re.Error).

$$\begin{aligned} Avg.Abs.Re.Error\,(\%) &= \frac{\sum_{t=1}^{T} Error(t)}{T} \times 100\% \\ where \quad Error(t) &= \frac{|\,R_{Pred} - R_{Exp}\,|}{R_{Exp}}, \\ t = index\,of\,test,\; T &= total\,No.\,of\,tests \end{aligned} \tag{5}$$

Results

Table 2: Model Fitting Results

Drop Size 10/1 pL	Drop Space μm	RMSE (%) For LSQR	
		Normalized	Re-scaled
10 pL	40 (635 dpi)	1.63	15.49
	25 (1016 dpi)	5.14	36.30
	20 (1270 dpi)	1.31	7.45
1 pL	25 (1016 dpi)	1.02	8.98
	20 (1270 dpi)	3.61	28.91
	10 (2540 dpi)	1.94	11.03
Average		**2.83**	**21.02**

The model fitting results are shown in the Table 2. The cross-validation result is shown in Figure 8. All the data (including the sheet resistance measurement data) are normalized to the range of [0,1] before the training and testing process. The RMSE (%) for the normalized data in the table listed above is calculated with the normalized sheet resistance. And the RMSE (%) for the rescaled data in the table listed above is calculated with the sheet resistance data that are rescaled from range of [0,1] to the original measurement range.

Judging the acceptable sensors is vital based on the prediction module mentioned in previous sections. It is defined that the acceptable electrodes are the electrodes with the sheet resistance values ranged within 1.5 standard deviation based on the measured sheet resistance data for each electrode printed with same set of parameters. The predicted acceptable electrodes are the electrodes with the sheet resistance values ranged within 1.5 standard deviation based on the predicted sheet resistance data for each electrode printed with same set of parameters. Based on the module introduced in previous section, the prediction of the acceptable electrodes is as accurate as 87%.

Conclusion

From results shown for the five-fold cross validation, the average absolute relative error is around 26%. Because the sheet resistance measurements are normalized before the training and testing process using a logarithmic method which causes a higher

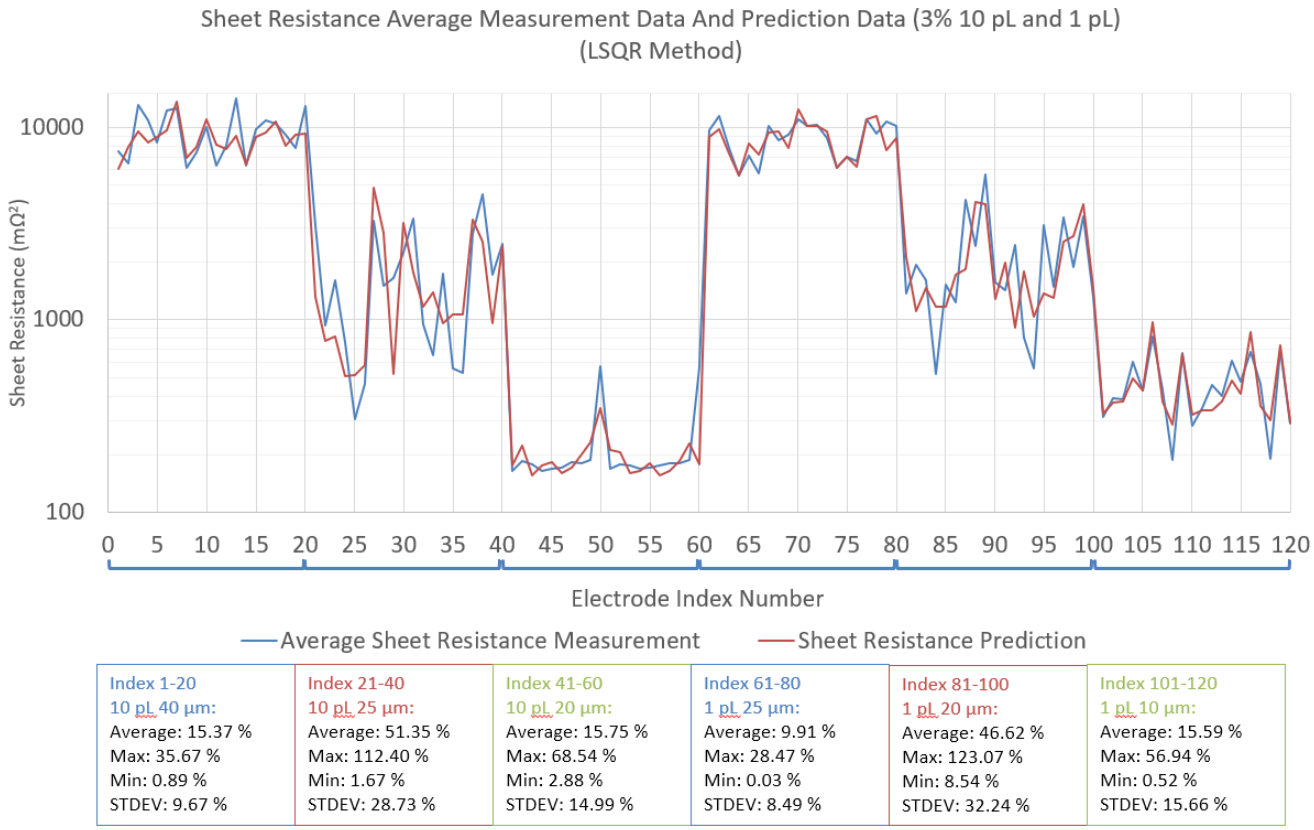

Figure 8. *Cross-Validation Trained and Tested with Least Squares Method: Original Experimental and Re-scaled Predicted Sheet Resistance*

degree of compression, the models give a relatively small error (average error is 21%) in the model fitting process. On the other hand, the results for the five-fold cross-validation (average error is 26%) are not as good as they appear in model fitting process.

While predicting sheet resistance with good accuracy is valuable, the method provides a non-contact, in-situ heuristic that can be generalized to monitor quality in a wide range of reel-to-reel applications Once trained, the model requires no further experiment measurement.

Considering that the main purpose of the sheet resistance prediction is to evaluate the quality of inkjet printed electrodes, determining whether the quality of the printing job is acceptable or not is more essential compared to the accuracy of the sheet resistance measurement. A further step for this investigation can be setting a threshold range regarding the features extracted from the images of the inkjet printed electrodes, and to judge whether the electrodes are acceptable.

References

[1] K.C. Chung, H.N. Cho, M.S. Gong, Y.S. Han, J.B. Park, D.H. Nam, S.Y. Uhm, and Y.K. Seo, Organic silver complexes, their preparation methods and their methods for forming thin layers," Jul. 24 2012, US Patent 8,226,755.

[2] J. A. Seibert, J. M. Boone, and K. K. Lindfors, Flat-field correction technique for digital detectors, in Medical Imaging 1998: Physics of Medical Imaging, vol.3336. International Society for Optics and Photonics, 1998, pp. 348-355.

[3] O. R. Vincent, O. Folorunso et al., A descriptive algorithm for Sobel image edge detection, in Proceedings of Informing Science & IT Education Conference (InSITE), vol. 40. Informing Science Institute California, 2009, pp. 97-107.

[4] N. Otsu, A threshold selection method from gray-level histograms, IEEE Transactions on Systems, Man, and Cybernetics, vol. 9, no. 1, pp. 62-66, 1979.

[5] D. Arthur and S. Vassilvitskii, k-means++: The advantages of careful seeding, in Proceedings of the Eighteenth Annual ACM-SIAM Symposium on Discrete Algorithms. Society for Industrial and Applied Mathematics, 2007, pp. 1027-1035.

[6] H. S. Fairman, M. H. Brill, and H. Hemmendinger, How the CIE 1931 colormatching functions were derived from Wright-Guild data," Color Research & Application: Endorsed by Inter-Society Color Council, The Colour Group (Great Britain), Canadian Society for Color, Color Science Association of Japan, Dutch Society for the Study of Color, The Swedish Colour Centre Foundation, Colour Society of Australia, Centre Français de la Couleur, vol. 22, no. 1, pp. 11–23, 1997.

[7] S. Lloyd, Least squares quantization in PCM, IEEE Transactions on Information Theory, vol. 28, no. 2, pp. 129-137, 1982.

[8] J. Grice and J. P. Allebach, The print quality toolkit: an integrated print quality assessment tool, Journal of Imaging Science and Technology, vol. 43, no. 2, pp. 187-199, 1999.

[9] E. H. Adelson, C. H. Anderson, J. R. Bergen, P. J. Burt, and J. M. Ogden,Pyramid methods in image processing, RCA Engineer, vol. 29, no. 6, pp. 33-41, 1984.

[10] T. Ojala, M. Pietikäinen, and T. Mäenpää, Multiresolution gray-scale and rotation invariant texture classification with local binary

patterns, IEEE Transactions on Pattern Analysis & Machine Intelligence, no. 7, pp. 971-987, 2002.

[11] M. Turtinen M. Pietikäinen, O. Silvén, T. Mäenpää, and M. Niskanen, Paper characterisation by texture using visualisation-based training, The International Journal of Advanced Manufacturing Technology, vol. 22, no. 11–12, pp. 890-898, 2003.

[12] T. Ahonen, A. Hadid, and M. Pietikäinen, Face recognition with local binary patterns," in European Conference On Computer Vision. Springer, 2004, pp. 469–481.

[13] C. C. Paige and M. A. Saunders, LSQR: An algorithm for sparse linear equations and sparse least squares, ACM Transactions on Mathematical Software (TOMS), vol. 8, no. 1, pp. 43-71, 1982.

[14] R. Barrett, M. W. Berry, T. F. Chan, J. Demmel, J. Donato, J. Dongarra V. Eijkhout, R. Pozo, C. Romine, and H. Van der Vorst, Templates for The Solution of Linear Systems: Building Blocks for Iterative Methods. SIAM, 1994, vol. 43.

[15] R.E. Fan, P.H. Chen, and C.J. Lin, Working set selection using second order information for training support vector machines," Journal Of Machine Learning Research, vol. 6, no. Dec, pp. 1889–1918, 2005.

[16] Yan, Yang, and Allebach, Jan P. (2019). Image-Based Non-Contact Conductivity prediction for Inkjet Printed Electrodes and follow-up work of toner usage prediction for laser electro-photographic printers, Theses and Dissertations Available from ProQuest.

Author Biography

Yang Yan received her B.S. (2016) and M.S. (2019) in Electrical Engineering from Purdue University. Her primary area of research has been image processing, image quality evaluation, and machine learning.

Qingyu Yang received her B.S.(2017) in Electrical Engineering from Purdue University and currently is a Ph.D. student from Purdue ECE. Her research focuses on image quality analysis, computer vision, objective detection and deep learning applications.

Kerry Maize received his B.S. in Electrical Engineering and Computer Science from UC Berkeley in 2002. He came to UCSC in 2005 to pursue graduate study in the areas of quantum electronics and nanoscience. His current work is focused on optical coherence tomograohy and thermal device characterization. Prior to engineering Kerry worked in journalism.

Jan P. Allebach is Hewlett-Packard Distinguished Professor of Electrical and Computer Engineering at Purdue University. Allebach was named Electronic Imaging Scientist of the Year by IS&T and SPIE, and was named Honorary Member of IS&T, the highest award that IS&T bestows. He has received the IEEE Daniel E. Noble Award, the IS&T/OSA Edwin Land Medal, is a Fellow of the National Academy of Inventors, and is a member of the National Academy of Engineering.

Ali Shakouri is a Professor of Electrical and Computer Engineering and Director of Birck Nanotechnology Center at Purdue University. He received his Ph.D. from Caltech. His current research is on nanoscale heat transport and electrothermal energy conversion. He has developed lock-in imaging for temperature measurement and for real-time monitoring of functional film manufacturing. He is also leading a team to manufacture low-cost smart internet of things (IoT) devices and sensor networks for applications in advanced manufacturing and agriculture.

George T. Chiu is a Professor of Mechanical Engineering with courtesy appointments in Electrical and Computer Engineering and Psychological Sciences at Purdue University. He received the B.S. degree from National Taiwan University and the M.S. and Ph.D. degrees from University of California at Berkeley. His research interests are mechatronics and control with applications to digital printing and imaging systems, digital fabrications and functional printing. He is a Fellow of ASME and IS&T.